Available online at www.sciencedirect.com

ScienceDirect

Procedia Manufacturing 29 (2019) 435–442

Procedia MANUFACTURING

www.elsevier.com/locate/procedia

18th International Conference on Sheet Metal, SHEMET 2019

Analysis of mechanical behaviour of AA6082-T6 sheets deformed at low temperatures

Stefania Bruschi*, Rachele Bertolini, Enrico Simonetto, Andrea Ghiotti

[a] *Department of Industrial Engineering, University of Padova, Via Venezia 1, 35131, Padova, Italy*

Abstract

High-resistant 6xxx series aluminium alloy sheets are more and more used in the automotive industry thanks to their high strength-to-density ratio, which allows the vehicles weight reduction; however, they can be hardly deformed at room temperature due to their reduced formability, while forming at elevated temperature usually leads to a reduction of the sheet strength, making necessary post-forming heat treatments. The present research study aims at evaluating the mechanical behaviour of AA6082-T6 sheets deformed in the temperature range between 300°C and -100°C, to assess the possible increase of both ductility and strength when deforming below room temperature. Uniaxial tensile tests were carried out at different temperature regimes and then, ductility, strength and failure mode were evaluated. Surface integrity after mechanical processing was investigated in terms of microstructures and nano-hardness measurements. Results confirmed that the strength and ductility of aluminium alloys improved at temperature decrease. Additionally, sheets deformed at low temperature were characterized by enhanced nano-hardness.

Keywords: Aluminum alloy; Cryogenic forming; Ductility; Hardening

* Corresponding author. Tel: +39 049 8276821.
E-mail address: stefania.bruschi@unipd.it

10.1016/j.promfg.2019.02.159

1. Introduction

In the last decade, the attention of the automotive field for producing panel components made of 6xxx series aluminum alloys has drastically increased thanks to the characteristics they offer, namely the high ratio between the strength and mass and good corrosion resistance, especially when provided in the T4 and T6 precipitation hardened states. However, the formability of such alloys when subjected to conventional stamping processes carried out at room temperature is quite low, limiting the geometrical complexity of the components that can be formed. Different approaches have been exploited to overcome this limitation, the most widespread being the conduction of heat-assisted forming processes [1]. In this framework, the initial blank can be heated to a working temperature sufficiently high to ensure a suitable formability increase, in the range of either warm [2] or hot forming [3] temperatures. Otherwise, the blank can be subjected to the so-called Hot Form and Quench HFQ™ process, where it is formed and quenched between cooled dies at elevated temperature after the solubilization treatment [4]. The HFQ™ process assures outstanding ductility and negligible springback, but forces to carry out an additional ageing treatment to maximize the formed component strength.

With the aim of preserving the component strength, but still assuring a sufficient ductility increase, the deformation process can be carried out at temperatures lower than the room one, which results in higher dislocation density, with a consequent strain hardening increase and decrease of strain localization that quickly leads to fracture [5]. Furthermore, in case of 5xxx series aluminum alloys, forming at low temperatures reduces the impact of the Portevin-Le Chatelier effect, which manifests itself with undesirable deformation bands on the formed component [6].

In this context, the objective of the paper is to evaluate the behaviour of AA6082-T6 sheets during and after deformation at low temperatures: for doing that, uniaxial tensile tests were carried out till -100°C, recording the material flow stress, as well as the strain at uniform elongation and fracture. For sake of comparison, the tensile tests were also carried out at room temperature and at temperatures typical of warm forming. Afterwards, nano-hardness measurements were conducted to evaluate the post-deformation strength as a function of the testing temperature. Furthermore, microstructural and surface fracture analyses were carried out to explain the material behaviour at different temperatures.

2. Experimental

2.1. Material

The material object of the investigation is the AA6082-T6 aluminum alloy provided in sheets of 1.5 mm of thickness, currently used in the automotive field for its good mechanical properties and excellent corrosion resistance. The nominal chemical composition and main mechanical properties of the alloy in the as-delivered condition are reported in Table 1 and Table 2, respectively.

Table 1. AA6082-T6 nominal chemical composition (wt%).

Si	Fe	Cu	Mn	Mg	Zn	Ti	Cr	Al
0.7-0.13	0.0-0.5	0.0-0.1	0.4-1.0	0.6-1.2	0.0-0.2	0.0-0.1	0.0-0.25	Balance

Table 2. AA6082-T6 mechanical properties in the as-delivered condition.

$Y_{0.2}$ (MPa)	UTS (MPa)	Hardness (HV)	Max Elongation (%)
260	310	100	11

2.2. Uni-axial tensile tests

Uni-axial tensile tests were carried out on a MTS™-322 hydraulic wedge, equipped with an environmental chamber allowing to control the testing temperature in a range from –130 (±2) °C to 315 (±2) °C (see Fig. 1 a). The AA6082-

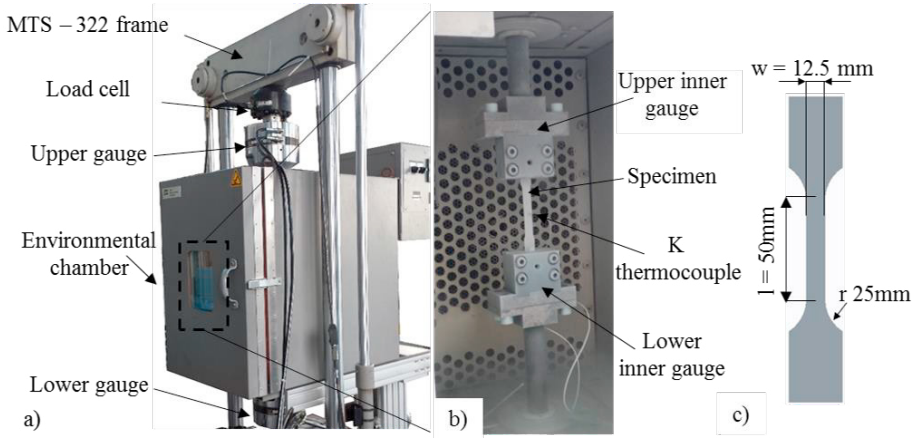

Fig. 1. Experimental equipment for tensile tests: (a) equipment overview; (b) environmental chamber detail; (c) specimen geometry.

T6 specimens were laser-cut from the provided sheets along the rolling direction with the geometry shown in Fig. 1 c, according to the ISO 6892 standard [7]. Even though sheet anisotropy may influence formability [8], the analysis carried out in this research work is focused on the material behavior along the rolling direction to give a preliminary assessment of possible advantages in low-temperature forming processes.
A k-thermocouple was spot-welded on each specimen to control and monitor the temperature during the test (see Fig. 1 b), while the inner gauges and the environmental chamber were kept at the testing temperature for 1 hour before loading the specimen in order to avoid non-homogenous thermal distributions. The tests were carried out at a strain rate equal to 0.1 s^{-1} and at 5 different temperatures, namely -100°, -50°, 25°, 200°, 250° and 300°C.

2.3. Post-deformation microstructural and mechanical analyses

After tensile testing, the specimen fracture surfaces were analyzed using both a FEI™ QUANTA 450 Scanning Electron Microscope (SEM) and Sensofar™ Plu-Neox 3D optical profiler. The former was used to provide qualitative information of the fracture typology: different images were recorded at a magnification of 1000x using the Secondary Electron (SE) probe. The latter was instead used to provide quantitative information: different surface roughness parameters, namely the arithmetical mean height of the surface *Sa*, the root mean square height of the surface *Sq*, and the maximum peak height *Sp*, were considered according to [9]. The surface topography measurements were taken by scanning the entire area of fracture by means of a 20x magnification Nikon™ confocal objective.

After mechanical processing, the specimens deformed at -100°C, 25°C and 300°C were prepared for metallographic observations: after cold mounting, grinding and polishing, the Keller's etchant was used to reveal the grain boundaries. The microstructure was observed using both a Leica™ DMRE optical microscope equipped with a high definition digital camera and the FEI™ QUANTA 450 SEM. On the same specimens, nano-indentation measurements were carried out using the iMicro™ from Nanomechanics Inc. nano-indenter to evaluate the nano-hardness after thermo-mechanical processing. A diamond Berkovich tip was used for all the tests. A number of ten indentations were performed using a load of 25 mN and a strain rate of 0.2 s^{-1} on different zones across the sections of each sample. Indentations were spaced sufficiently far apart so that the indentation behaviour was not affected by the presence of adjacent indentations, in accordance with the ISO 14577-4:2016 standard [10].

Differential Scanning Calorimetry (DSC) measurements were finally performed using a DSC Q200™ differential scanning calorimeter to provide information about the precipitation state of the alloy after thermo-mechanical processing. The specimens were continuously heated up to 500°C with a heating rate of 5°C/min. For sake of comparison, also the sheet in the as-delivered condition was tested.

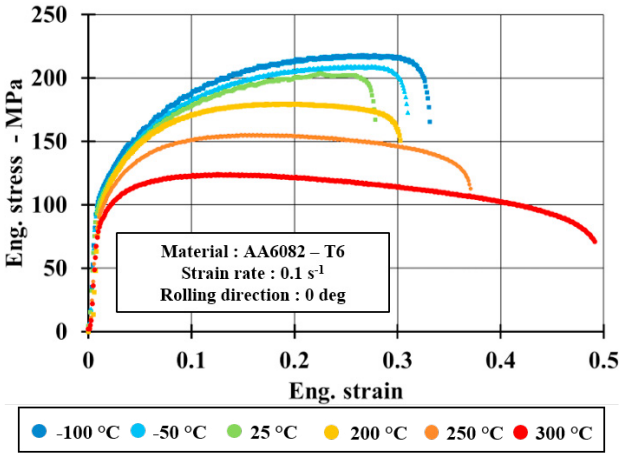

Fig. 2: Engineering flow curves for different testing temperatures at strain rate $0.1s^{-1}$.

3. Results and discussion

3.1. Strain hardening and ductility characteristics

Fig. 2 shows the AA6082-T6 engineering flow curves at varying temperature. As expected, testing at temperature higher than the room one leads to the flow stress decrease, whereas the opposite is observed when testing at temperatures lower than the room one. This trend is observed also for the Ultimate Tensile Stress (UTS) in Fig. 3 a, which monotonically decreases from -100°C to 300°C. The strain hardening exponent, calculated as the slope of the flow stress curve in the bi-logarithmical chart between the yield stress and UTS, is shown in Fig. 3 b, is the highest at the lowest testing temperature, and the lowest at 300°C, whereas it does not change significantly in between. This means that 300°C is the temperature at which the microstructural phenomenon of dynamic recovery becomes important, leading to dislocations annihilation and therefore softening. On the contrary, the highest hardening coefficient at -100°C helps in postponing strain localization, increasing the uniform elongation before necking, as shown in Fig. 4 a, where the engineering strain calculated at UTS at varying testing temperature is reported. The increase in uniform elongation at low temperature compared to room temperature is 18% on an average. Whereas, the uniform elongation is reduced when testing temperatures higher than the room temperature are applied, reaching the minimum at 300°C, with a percentage decrease equal to 45%. When evaluating the strain at fracture sensitivity to temperature (see Fig. 4 b), the low temperature testing still induces an increase of ductility, quantifiable in 4.7% at -100°C, even if the increase is much more significant at 250°C and 300°C, being 11% and 63%, respectively. This means that at the highest testing temperatures, the overall ductility increase is due to the post-necking elongation, with, therefore, significant strain localization. On the other hand, deforming at temperatures lower than the room one allows increasing uniform elongation, with, at the same time, an increase of strain hardening.

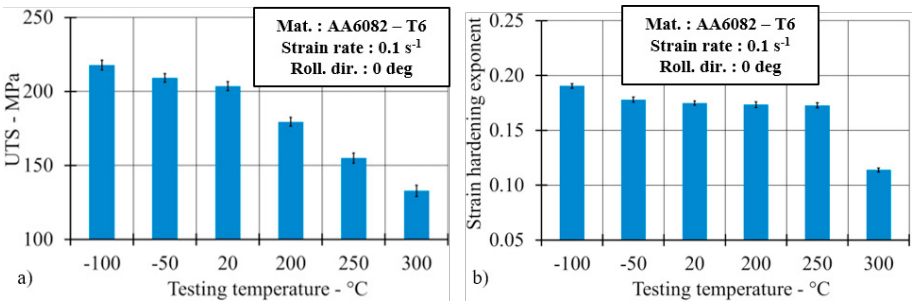

Fig. 3. (a) UTS and (b) strain hardening exponent at varying testing temperature.

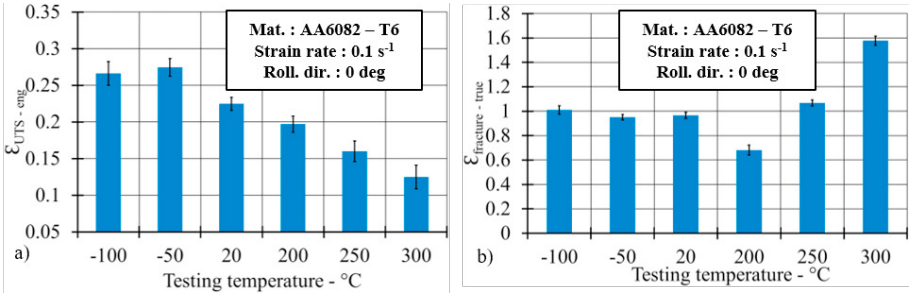

Fig. 4: (a) Engineering strain at UTS (b) True strain at fracture.

3.2. Post-deformation microstructural and mechanical features

The optical micrographs in Fig. 5 a show that all the deformed microstructures present equiaxed grains, with no significant grain coarsening at increasing testing temperature. Furthermore, the SEM micrographs in Fig. 5 b and c show that two types of intermetallic compounds are dispersed in all the deformed microstructures, which can be distinguished on the basis of their color, namely white and black. In particular, the white ones are commonly associated with AlFe(MnCr)Si intermetallic compounds, while the black ones with Al-Mg-Si intermetallic compounds [11]. Magnesium and silicon are the most important alloying elements of AA6082 since they form Mg_2Si, which increases the alloy strength.

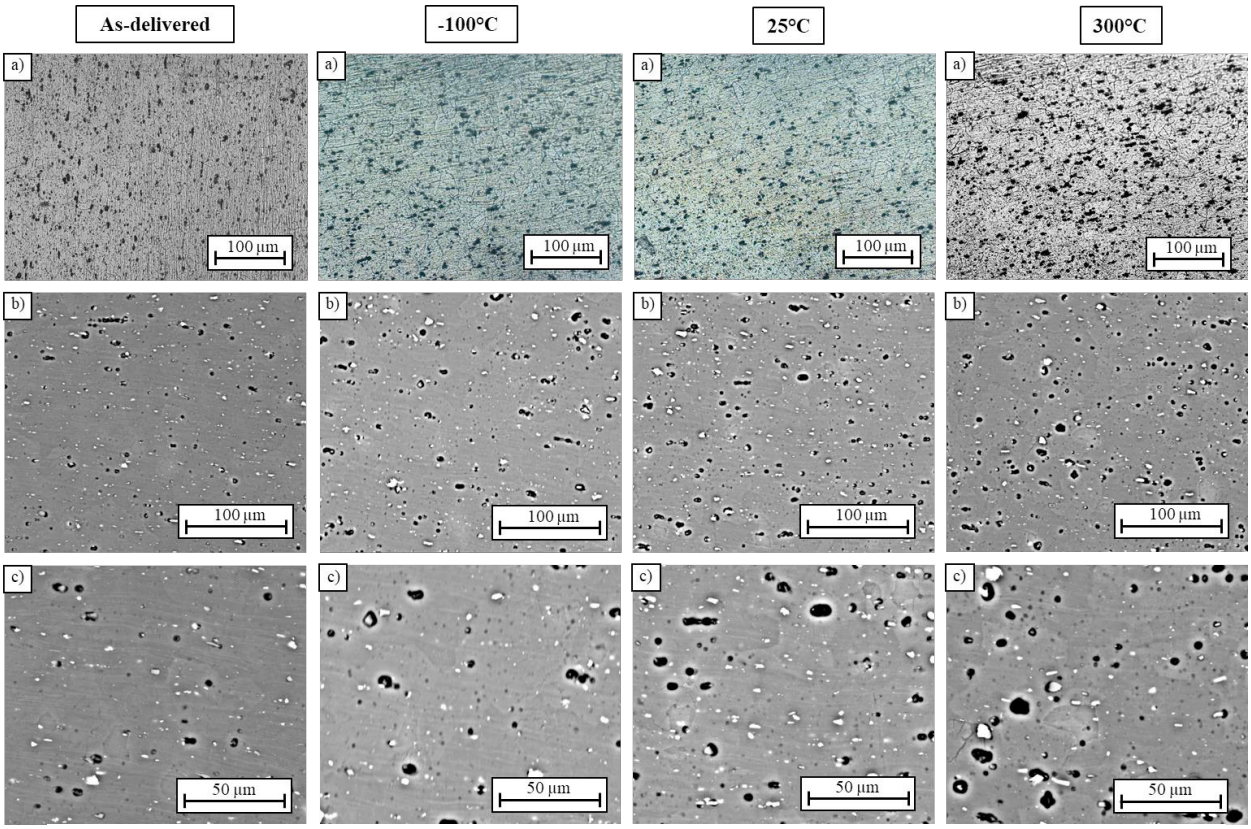

Fig. 5. (a) Optical and (b-c) SEM micrographs of the deformed specimens at varying testing temperature.

The fraction of silicon and/or magnesium that is not bound in Mg_2Si form with iron a consistent number of phases, which are described in details in [11]. The intermetallics influence on the mechanical properties depends on their composition, morphology, size and spatial distribution: in particular, finer intermetallics are usually associated to higher resistance. Even if the microstructure does not change, in terms of type of intermetallics, as a function of the testing temperature, a drastic change in their size is noticeable at increasing deformation temperature, as confirmed by the SEM images in Fig. 5 b and c. Actually, both types of intermetallic particles resulted larger in size at increasing testing temperature.

Data from nano-hardness measurements confirm the microstructural observations. Fig. 6 a, which reports the nano-hardness of the deformed specimens as a function of the testing temperature, shows that a nano-hardness increase after deformation is noticeable for those specimens deformed at -100°C and room temperature, with a percentage increment of 8% and 5% compared to the as-delivered alloy, respectively. On the contrary, softening leading to nano-hardness decrease of 9% compared to the base alloy is found for the specimen deformed at 300°C. This peculiar hardening behaviour at low temperatures can be ascribed to the fine size of intermetallic particles, which favors more effectively the dislocation hardening by pinning them and thus further enhancing the formation of dislocation cell networks within the deformed grains. This was also reported in [12], where the effect of severe plastic deformation processes on secondary phase particles of an Al-Mg-Si alloy was studied.

Fig. 6 b shows the DSC curves of the deformed samples. The curve relative of the sample in the as-delivered condition is also included for sake of comparison. The DSC curves for the AA6082 alloy, in the interval of considered temperatures, usually shows four peaks corresponding to the formation of aluminum cluster (70–120°C), the formation of Guinier-Preston zones (120-180°C), the precipitation of β'' (190–275°C), and β' phases (290–355°C), respectively. Among these, the β precipitates are considered to give the main contribution to strength and hence they are mostly responsible for the peak age hardening effect [13]. Fig. 6 b) clearly demonstrates that the exothermic peaks relative to the β'' and β' phases are shifted towards lower temperatures as the deformation temperature is reduced. Therefore, the precipitation kinetics results changed when the alloy structure is plastically deformed. This can be correlated to the amount of deformation stored in the specimen, since dislocations promote heterogeneous nucleation sites for precipitates [5]. The above mentioned results are in agreement with those of reported in Fig. 6a, which shows the highest hardness for specimens deformed at temperatures lower than the room one.

The present data are indeed in good agreement with established evidence showing that the kinetics of transition precipitates is deeply altered by deformation. Zhen et al. [14] showed that when Al-Mg-Si alloys had been extensively cold rolled, their aging curves featured a decrease of the precipitation temperatures of some phases. In [15], AA6061 and AA6063 alloys were subjected to room temperature and cryogenic rolling applying severe plastic deformation: it was observed that low-temperature processing caused a substantial suppression of structure recovery during straining and hence preserved higher dislocation densities in the specimens, increasing the driving force for sub-microcrystalline grain development.

Moreover, specimens deformed at 300°C show no peaks relevant to clusters and Guinier-Preston zones, together with a lower intensity of the β' and β'' peaks. This can be attributed to the annihilation of vacancies that is due to recovery and recrystallization, as confirmed by the strain hardening results reported in Fig. 3 b [15].

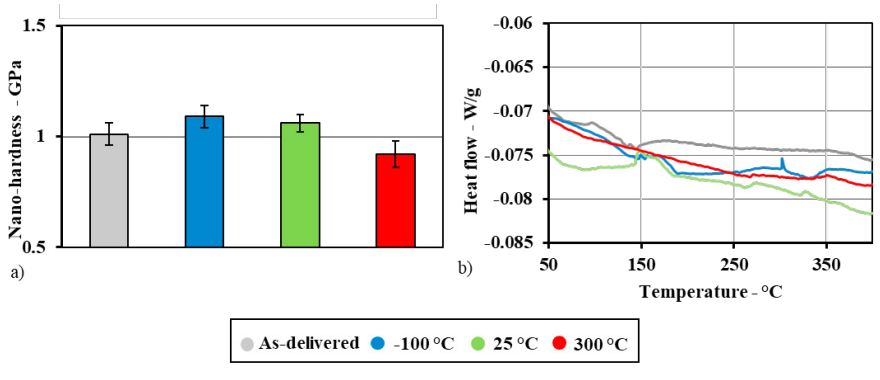

Fig. 6. (a) Nano-hardness; (b) DSC curves at varying testing temperature.

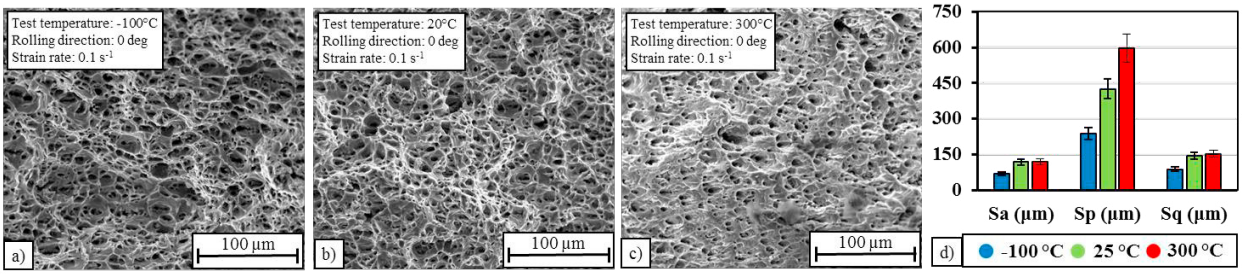

Fig. 7. (a-b-c) SEM fracture surfaces, and (d) areal parameters of the fracture surfaces at varying testing temperature.

Fig. 7 a-c shows the SEM fracture surfaces of the specimens deformed at -100°C, room temperature and 300°C, respectively: they all present the conventional ductile fracture morphology, characterized by the presence of dimples, randomly distributed. To have a further insight about the degree of ductility on the basis of the different testing temperatures, areal surface parameters were calculated from the acquired 3D topographies of the fracture surfaces. Fig. 7 d shows the influence of the testing temperature on 3 surface parameters that have been recognized to be related to the fracture surface ductility, namely the arithmetical mean height of the surface *Sa*, the height of the highest peak of the surface *Sp*, and the root mean square height of the surface *Sq*. It is worth noting that the fracture surface of the specimen tested at -100°C always shows the lowest values of the considered parameters, even if the strain at fracture value is comparable to that of the specimen deformed at room temperature (see Fig. 4 b). On the contrary, whereas the *Sa* and *Sq* values of the specimens deformed at room temperature and 300°C are similar, the difference of the *Sp* values is much more significant, meaning that the *Sp* parameter is the most sensible to the ductility characteristics.

4. Conclusions

In this paper AA6082-T6 specimens were subjected to uniaxial tensile testing in a wide range of temperatures, from -100°C to 300°C. The main following conclusions can be drawn:

- Deforming at temperatures lower than the room one assured higher flow stress and strain hardening, together with higher uniform elongation, whereas deforming at 300°C assured higher post-necking deformation.
- Nano-hardness of specimens deformed at temperatures lower than the room one was higher as a consequence of the presence of finer intermetallic particles.
- Regardless of the deformation temperature, the fracture surfaces always presented ductile characteristics, with a different degree of ductility as proved by the 3D profiler quantitative measurements.

References

[1] K. Zheng, D.J. Politis, L. Wang, J. Lin, A review on forming techniques for manufacturing lightweight complex-shaped aluminum panel components, International Journal of Lightweight Materials and Manufacture,1(2) (2018) 55-80.
[2] R. Neugebauer, T. Altan, M. Geiger, M. Kleiner, A. Sterzing, Sheet metal forming at elevated temperatures, CIRP Annals – Manufacturing Technology, 55 (2) (2006) 793-816.
[3] P.F. Bariani, S. Bruschi, A. Ghiotti, F. Michieletto, Hot stamping of AA5083 aluminum alloy sheets, CIRP Annals – Manufacturing Technology, 62 (1) (2013) 251-254.
[4] M.S. Mohamed, A.D. Foster, J. Lin, D.S. Balint, T.A. Dean, Investigation of deformation and failure features in hot stamping of AA6082: Experimentation and modelling, International Journal of Machine Tools and Manufacture, 53 (1) (2012) 27-38.
[5] M. Kumar, N. Sotirov, F. Grabner, R. Schneider, G. Mozdzen, Cryogenic forming of AW-6016-T4 sheet, Trans. Nonferrous Soc. China, 27 (2017) 1257-1263.
[6] N. Sotirov, G. Falkinger, F. Grabner, G. Schmidt, R. Schnieder, R.J. Grant, R. Kelsch, K. Radlmayr, M. Scheerer, C. Reichl, H. Sehrschon, M. Loipetsberger, Improved formability of AA5182 aluminium alloy sheet at cryogenic temperatures, Materials Today: Proceedings 2S (2015) S113-S118.
[7] ISO 6892: Metallic materials -- Tensile testing -- Part 1: Method of test at room temperature.
[8] S.Bruschi, T. Altan, D. Barnabic, P.F. Bariani, A. Brosius, J. Cao, A. Ghiotti, M. Khraisheh, M. Merklein, A.E. Tekkaya, Testing and modelling of material behavior and formability in sheet metal forming, CIRP Annals – Manufacturing Technology, 63 (2014) 727 – 749.

[9] E. Merson, A. V. Kudrya, V. A. Trachenko, D. Merson, V. Danilov, A. Vinogradov, The Use of Confocal Laser Scanning Microscopy for the 3D Quantitative Characterization of Fracture Surfaces and Cleavage Facets, Structural Integrity Procedia, 2 (2016) 533–540.
[10] ISO 14577-4:2016 standard: Metallic materials -- Instrumented indentation test for hardness and materials parameters -- Part 4: Test method for metallic and non-metallic coatings
[11] M. Tercelj, M. Fazarinc, G. Kugler, I. Perus, Influence of the chemical composition and process parameters on the mechanical properties of an extruded aluminium alloy for highly loaded structural parts, Construction and Building Materials, 44 (2013) 781–791.
[12] S. Kumar Panigrahi, R. Jayaganthan, V. Pancholi, Effect of plastic deformation conditions on microstructural characteristics and mechanical properties of Al 6063 alloy, Materials and Design, 30 (2009) 1894–1901.
[13] M. Takeda, F. Ohkubo, T. Shirai, and K. Fukui, Stability of metastable phases and microstructures in the ageing process of Al-Mg-Si ternary alloys, J. Mat. Sci., 33 (1998) 2385–2390.
[14] L. Zhen, W. D. Fei, S. B. Kang, H. W. Kim, Precipitation behaviour of Al-Mg-Si alloys with high silicon content, J. of Mat Sci, 32 (1997) 1902-1997.
[15] S. K. Panigrahi, D. Devanand, R. Jayaganthan, A Comparative study on mechanical properties of ultrafine-grained Al 6061 and Al 6063 alloy processed by cryorolling. Trans Indian Inst Met, 61 (2008) 1–5.